Equivalent Circuit Model For Sodium-Ion Batteries With Physical-Based Representations Of Their Non-Linearities

Houssam Rabab, Nicolas Damay, Christophe Forgez, Asmae El Mejdoubi, Aurélien Quelin

Equivalent Circuit Model For Sodium-Ion Batteries With Physical-Based Representations Of Their Non-Linearities

Houssam Rabab
University of Technology of Compiègne
Compiègne, France

Nicolas Damay
University of Technology of Compiègne
Compiègne, France
nicolas.damay@utc.fr

Christophe Forgez
University of Technology of Compiègne
Compiègne, France

Asmae El Mejdoubi
Tiamat
Amiens, France

Aurélien Quelin
Tiamat
Amiens, France

***Abstract*—Sodium-ion batteries are a promising technology whose performance can meet the demand of the automotive sector. These batteries require a model that can predict accurately their non-linear behavior with respect to the state of charge. We modeled these cells using a modified equivalent circuit model, with an approach that can separate and study the different electrochemical phenomena involved. The model can accurately provide information on phenomena such as charge transfer and solid-electrolyte interphase. The model can also provide information on the diffusion of sodium within the electrodes or in the electrolyte at a state of charge above 30 percent.**

***Index Terms*—battery, Sodium ion, equivalent circuit model, state of charge, charge transfer, SEI, diffusion.**

I. Introduction

The inevitable transition from conventional to electric vehicles motivates researchers and companies to develop new battery technologies. After all, battery packs provide the total power output of an electric vehicle. Besides energy density, the automotive sector demands high power density batteries, especially for fast charging and regenerative breaking.

The sodium-ion batteries of the NVPF/HC type can meet the needs of electric and hybrid vehicles. These batteries offer a high power density and good stability [1], [2]. This battery has NVPF ($Na_3V_2(PO_4)_2F_3$) as positive electrode, and hard carbon HC as negative electrode.

Sodium-ion batteries have the same electrochemical phenomena present in lithium-ion technology. However, the effects of the electrochemical phenomena, in the NVPF/HC batteries, present strong non-linearities in the state of charge of the cell [3]. Therefore, a classical equivalent circuit model [4] (denoted ECM), whose parameters were adjusted with interpolation tables, can hardly keep up with the complexity of the effects of the electrochemical phenomena [5].

In this paper, we proposed a new approach to model NVPF/HC batteries based on a modified ECM. This approach aims at predicting accurately the non-linearities of the electrochemical phenomena present in these cells. The model will be composed of four contributions that will represent the different electrochemical phenomena. The parameters of each contribution were characterized using physical laws instead of interpolation tables. This is because interpolation tables require a tremendous number of tests [6]. Moreover, these tables are heavy since they need to be at least four-dimensional to track the impact of current, temperature, state of charge (denoted SoC) and state of health. Also, the parameters characterization should not rely on complex equations, since the model should be embedded in a battery management software (denoted BMS).

First, we will present the modified ECM. Next, we will describe the experimental protocol used for the characterization of the model parameters. After, we will detail the characterization of the parameters in the form of two sub-models: surface model and diffusion model. Finally, we will present the results obtained by the model.

II. Battery Model

Equation (1) represents the ECM taking into account its current I, temperature T and SoC dependencies. The ECM is illustrated by Fig. 1, where we split the cell voltage into four contributions.

$$\begin{aligned} U_{cell}(I,T,SoC) &= SEV(I,T,SoC) + V_s(I,T) \\ &+ V_{surf}(I,T,SoC) + V_{ld}(I,T) \end{aligned} \tag{1}$$

A. Surface equilibrium voltage and solid diffusion contribution

The first contribution is the surface equilibrium voltage [7], denoted SEV and represented by a voltage source in Fig. 1. Equation (2) presents the relation between SEV as a shift of the open circuit voltage (denoted OCV) in SoC. This shift in SoC represents the effects of the solid diffusion, which is the diffusion of sodium within each electrode. The effect of solid diffusion is expressed by the "shift in SoC" parameter (denoted ΔSoC_{sd}). We will explain in section V the reason to model the solid diffusion through the OCV.

$$SEV(I,T,SoC) = OCV(SoC + \Delta SoC_{sd}(I,T)) \tag{2}$$

Work funded by Région Hauts-de-France and Tiamat Energy

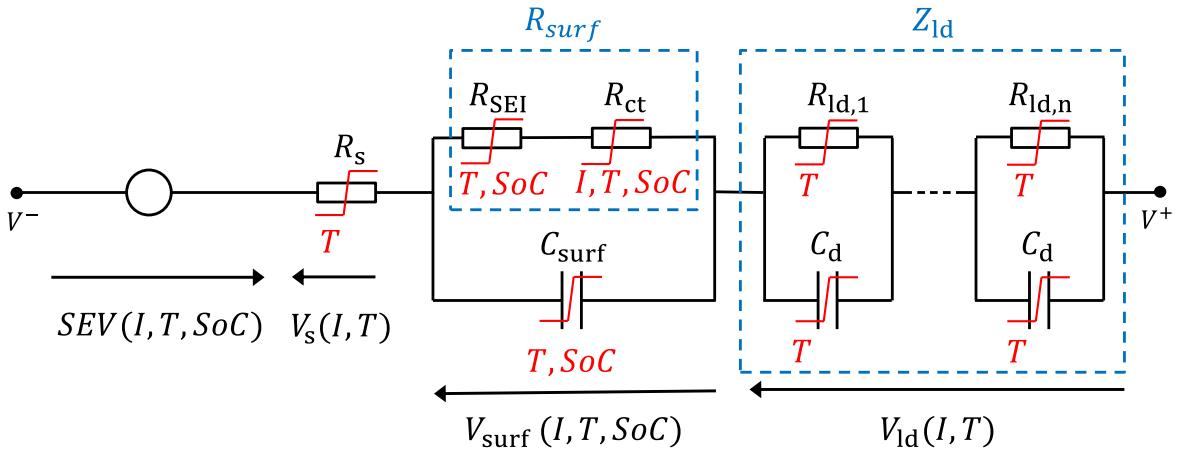

Fig. 1. Equivalent circuit model.

B. Static contribution

The second contribution is the voltage drop due to static phenomena, denoted V_s, such as the resistance of each component in the cell. These phenomena are represented by the series resistance R_s.

C. Surface contribution

The third contribution is the voltage drop due to the fast dynamic phenomena, denoted V_{surf}. These phenomena occur between the interface of the electrodes and the electrolyte, such as charge transfers and the solid electrolyte interphase (SEI). These phenomena will be called the surface phenomena in this article. They are represented by a first-order $R_{surf}//C_{surf}$ circuit. The parameters to be characterized are: the charge transfers resistance R_{ct}, the SEI resistance R_{SEI} and the time constant $\tau_{surf} = R_{surf} \cdot C_{surf}$. R_{surf} is called the surface resistance, which is the sum of R_{ct} and R_{SEI}.

D. Liquid diffusion contribution

The fourth contribution is the voltage drop due to the effect of the liquid diffusion, which is the diffusion of the sodium ion in the electrolyte. The liquid diffusion is represented by the voltage drop V_{ld}, which is the voltage of the n order $R_{ld,i}//C_d$ circuit. The dynamics of solid and liquid diffusion are assumed to be equal and are related to the same diffusion time constant $\tau_d = R_{ld} \cdot C_d$, where R_{ld} is the equivalent resistance of all $R_{ld,i}$. τ_d is assumed independent of SoC [8].

III. Experimental protocol

In this section, we present the tests required for characterizing the ECM parameters. We used a single 18650 NVPF/HC battery provided by Tiamat. Its nominal capacity is 700 mAh.

The aim is to use a minimum amount of measurements without reducing the accuracy of the model. For this, we use three types of tests:

- Electrochemical impedance spectroscopy tests, denoted EIS tests, at SoC 80%, 30% and 20%. These tests were used to determine $R_s(T)$, $\tau_{surf}(T, SoC)$ and $R_{surf}(I \approx 0, T, SoC)$;
- Short pulse tests (20 s) at charge and discharge mode. Each discharge pulse was followed by a charge pulse so that the same SoC remains at the end of these tests [3]. These tests were used to characterize $R_{surf}(I, T, SoC)$ at non-zero currents. The tests were taken at SoC 80%, 30% and 20%;
- Constant current tests between SoC 0% and 100%, with one-hour pause when the SoC is at near 60%. The pause is applied to properly determine τ_d (which corresponds to the resumption behavior of the cell after the one-hour pause at a SoC of around 60%). These tests were used to characterize $\Delta SoC_{sd}(I, T)$, $R_{ld}(T)$ and $\tau_d(T)$.

In order to study the non-linearity in temperature, these tests were conducted at three temperatures: 25 °C, 10 °C and 5 °C.

IV. Surface model

This section details the parameters characterization of the surface phenomena. These phenomena include charge transfers, SEI and double layer capacitance. The impact of these phenomena is critical particularly when the SoC is in the 0% to 30% range [3]. Therefore, our model must properly fit the voltage drops V_{surf} to ensure its reliability as much as possible, especially at low SoC.

Another purpose of the model is to diagnose the effects of the surface phenomena. Therefore, the model is designed in such a way that it is able to separate the surface phenomena into two:

- the charge transfers effects, by characterizing the non-linear resistance R_{ct}. This parameter depends on current, temperature and SoC;
- the SEI effects, by characterizing R_{SEI}. This parameter depends on temperature and SoC.

The dynamics of surface phenomena is modeled by the surface time constant τ_{surf}.

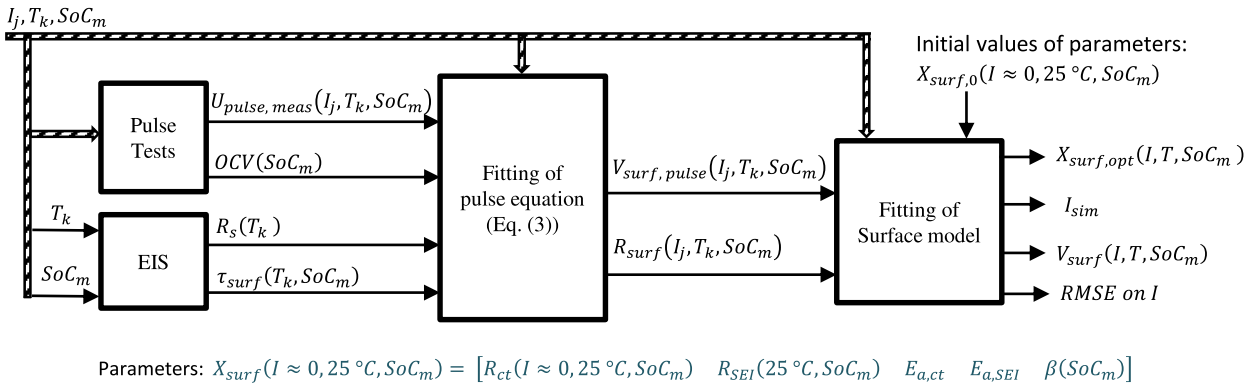

Fig. 2. Flowchart for characterizing surface model parameters.

A. Characterization

Fig. 2 represents the steps for characterizing the parameters R_{ct}, R_{SEI} and τ_{surf}.

First, we realized tests at precise temperatures T_k (5 °C, 10 °C and 25 °C) and SoC_m (20%, 30% and 80%). Based on the pulse tests at several current I_j , we had voltage measurements $U_{pulse,meas}(I_j, T_k, SoC_m)$ at different currents I_j, different temperatures T_k and different states of charge SoC_m. In addition, we used EIS tests to determine $R_s(T_k)$ and $\tau_{surf}(T_k, SoC_m)$.

Then, since we made pulses with short durations (20 seconds), the behavior of the diffusion effects corresponds well to the semi-infinite conditions of a Warburg impedance [9], [10]. This implies that for a short duration, the cell voltage can be represented by (3). Namely, ΔV_W is the Warburg voltage used in Fick's laws and U_i is the cell voltage at the first instant of the pulse.

$$U_{pulse,meas}(t) = U_i(t) + (R_s + R_{surf})I(t) + \Delta V_W(t) \quad (3)$$

The second step consists in extracting $V_{surf,pulse}(I_j, T_k, SoC_m)$ (see (4)) and $R_{surf}(I_j, T_k, SoC_m)$ by performing a fit via (3). Since we neglect the transient part of the surface phenomena, the fitting error is considered between $t = 3\tau_{surf}(T_k, SoC_m)$ and the end of the pulse duration.

$$V_{surf,pulse}(t) = R_{surf} \cdot I(t) \quad (4)$$

The third step is to separate $R_{surf}(I_j, T_k, SoC_m)$ into $R_{ct}(I_j, T_k, SoC_m)$ and $R_{SEI}(T_k, SoC_m)$. This is feasible by adopting the surface model proposed by Damay *et al.* [11]. This model uses the Butler-Volmer equation (see (5)), where I_0 is the exchange current density, β is the symmetry coefficient, F is the Faraday's constant, R is the gas constant, T is the temperature, I is the current simulated by the surface model (noted I_{sim} in Fig. 2) and V_{ct} is the charge transfers voltage which is calculated using (6). Equation (5) describes the dependence of R_{ct} on current. We also applied Arrhenius laws to describe the dependence of R_{ct} and R_{SEI} on temperature. In the original work [11], β was equal to 0.5. However, for this work, we kept β as a parameter to be determined.

$$I = I_0 \left[\exp\left(\frac{(1-\beta)F}{RT} V_{ct} \right) - \exp\left(\frac{-\beta F}{RT} V_{ct} \right) \right] \quad (5)$$

$$V_{ct} = V_{surf,pulse} - R_{SEI} \cdot I \quad (6)$$

The surface model has five parameters: R_{ct}(I≈0, 25 °C, SoC_m), R_{SEI}(25 °C, SoC_m), $E_{a,ct}$, $E_{a,SEI}$ and $\beta(SoC_m)$. These parameters are referred as $X_{surf}(SoC_m)$ in Fig. 2. $E_{a,ct}$ and $E_{a,SEI}$ are respectively the activation energies of charge transfers and the SEI, these two parameters are used in Arrhenius equations. Using these parameters, we can predict the effects of charge transfers and SEI for any current and any temperature, at a given SoC.

We fit these parameters in such a way that the simulated current I_{sim} is as close as possible to the measured current I_j, i.e. in the case where the root mean squared error on current (RMSE on I) is minimal. This can be done using the fmincon function in Matlab.

The obtained optimized parameters $X_{surf,opt}(I, T, SoC_m)$ correspond to the three applied SoCs: 20%, 30% and 80%.

For the SoC dependency, R_{surf} is expressed as a function of SoC by the four-degree-of-freedom exponential equation (7). It is an empirical equation, determined by observational data. The coefficients A_{surf}, B_{surf}, C_{surf} and D_{surf} were obtained by fitting (7) to R_{surf} measurements at near-zero current at 25 °C.

$$R_{surf}(SoC) = A_{surf} + B_{surf} \cdot \exp\left(\frac{C_{surf} - SoC}{D_{surf}} \right) \quad (7)$$

B. Results

Fig. 3 shows the relationship between the voltage drop due to surface phenomena V_{surf} and the current. The three solid curves represent the V_{surf} simulated by the surface model at 25 °C (red), 10 °C (blue) and 5 °C (yellow). The circled points

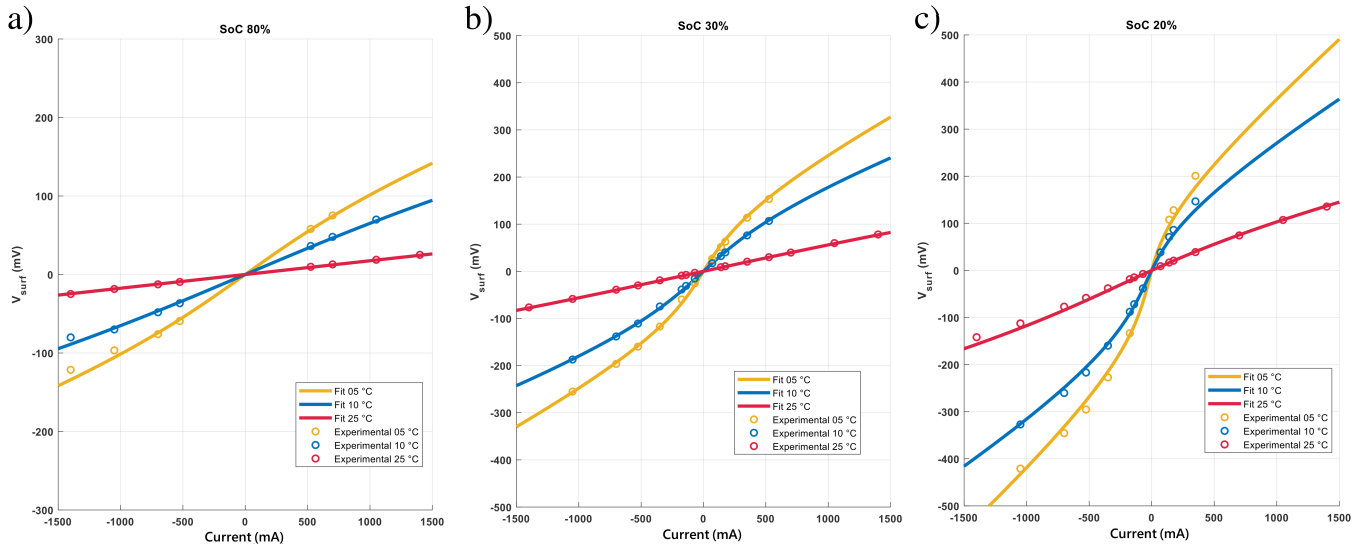

Fig. 3. Evolution of V_{surf} (continuous curves) and $V_{surf,pulse}$ (circled points) in function of current at 25 °C (red), 10 °C (blue) and 5 °C (yellow) at: a) SoC 80%, b) SoC 30%, c) SoC 20%.

represent the $V_{surf,pulse}$ obtained by the fit of the (3), which we considered as measurement points.

We can confirm that the surface model is applicable on NVPF/HC cells. The model manages to follow the measurement points for the three chosen SoCs and the three chosen temperatures, with RMSE on current equals to: 2.69% at SoC 80%, 2.87% at SoC 30% and 4.25% at SoC 20%. The importance of this model is that it manages to fit even in the low SoC areas (20% to 30%), as the effects of the surface phenomena have a significant impact in this area compared to the effects of the surface phenomena at higher SoC (above 40%) [3].

V. Diffusion Model

This part explains the parameters characterization of the slow dynamics phenomena represented by Z_{ld} and ΔSoC_{sd} (Fig. 1). In fact, NVPF/HC batteries feature electrodes whose diffusion of sodium varies non-linearly with the SoC. The effects of sodium diffusion have a significant impact especially when the SoC is in the range of 40% to 50%. This behavior is due to the gradient of NVPF potential in this range of SoC [12]. Therefore, we proposed a diffusion model that is able to separate the phenomena of slow dynamics into solid and liquid diffusion. This could allow the diagnosis of the diffusion effects in the electrolyte and in the two electrodes as well. It will also give information especially when another electrolyte or electrodes materials are used.

According to the work carried out by Kremer *et al.* [13] on LTO batteries, solid-state diffusion impacts the lithium concentration at the electrode surface c_{surf}, affecting the surface equilibrium potential (SEP) of the electrode. We propose to define a surface equilibrium voltage SEV which is the difference between the two electrodes SEP. The notion of equilibrium voltage is to be understood here as the equilibrium of the sodium-ion insertion reactions. This is different from the notion of classical OCV in ECMs, which corresponds to a global equilibrium of the cell: where chemical reactions are at equilibrium and all concentration gradients are relaxed.

Since we're working on a macroscopic scale, we don't have access to chemical information such as the surface sodium concentration on the electrodes. For this, we used the SoC concept. Mergo Mbeya *et al.* [14] proposed a relation between the SoC and the mean concentration c_{mean} in the electrodes of $LiFePO_4$/graphite cells. We propose to decompose c_{surf} into the sum of a mean concentration c_{mean} and a shift from the mean concentration Δc . The term c_{mean} is thus directly related to the cell SoC and the term Δc would thus correspond to a SoC shift due to solid diffusion ΔSoC_{sd}.

As a result, the macroscopic effect of the solid diffusion corresponds to a SoC shift of the OCV, that can be determined experimentally as presented in this paper (see section V.B). ΔSoC_{sd} is a dynamic value that depends on current and temperature. Please note that when the cell is at open-circuit, ΔSoC_{sd} tends towards zero and the SEV tends towards the OCV.

As for the effect of liquid diffusion, we modeled as a limited diffusion impedance [15]. According to Mauracher *et al.* [16], the effect of liquid diffusion does not exhibit non-linearities in SoC. Therefore, Z_{ld} depends only on temperature.

The dynamics of both solid and liquid diffusion is considered equal to τ_d and depends only on temperature.

A. Characterization

Fig. 4 represents the steps for characterizing the parameters ΔSoC_{sd}, R_{ld} and τ_d.

The first step is to extract the temporal evolution of the measured cell voltage $U_{cell,meas}$ for different I_j and T_k. These measurements were obtained by the constant current tests mentioned in section III.

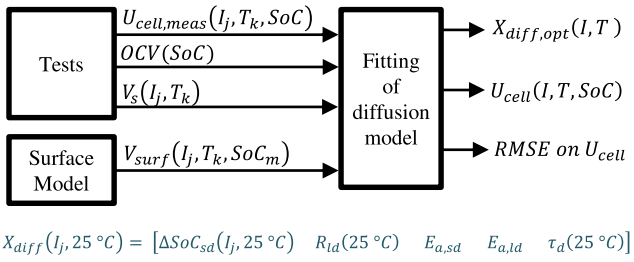

Fig. 4. Flowchart for characterizing diffusion model parameters.

The second step is to fit U_{cell} (obtained in (1)) to the measured voltage $U_{cell,meas}$. $V_s(I_j, T_k)$ is already determined by the EIS tests used to get $R_s(T_k)$, $V_{surf}(I_j, T_k, SoC_m)$ is simulated by the surface model presented in section IV, and the $OCV(SoC)$ is measured by a constant current test at 70 mA (C/10). Therefore, we have just these parameters to fit: $\Delta SoC_{sd}(I_j, T_k)$, $R_{ld}(T_k)$ and $\tau_d(T_k)$. We applied a fit at the cell voltage level. To do so, we used the fmincon function to characterize the parameters by minimizing the RMSE between the simulated cell voltage U_{cell} and the measured cell voltage $U_{cell,meas}$.

For the current dependency, ΔSoC_{sd} is characterized by a simple linear equation (see (8)). The term Q_{cell} refers to the battery nominal capacity which is 0.7 Ah. The coefficients k_1 and k_2 were adjusted during the fit of (1).

$$\Delta SoC_{sd}(I, 25\ °C) = k_1 \cdot I/Q_{cell} + k_2 \tag{8}$$

For the temperature dependency, we applied the Arrhenius law on ΔSoC_{sd} and R_{ld}. Thus, we got two additional parameters to be fit, which are the activation energies of solid and liquid diffusion, noted $E_{a,sd}$ and $E_{a,ld}$ respectively.

Finally, the model gives us the following three informations: $\Delta SoC_{sd}(I, T)$, $R_{ld}(T)$ and $\tau_d(T)$. In Fig. 4, X_{diff} refers to the diffusion parameters and $X_{diff,opt}$ refers to the optimal values of the diffusion parameters obtained via fitting.

B. Results

Fig. 5 shows the evolution of the voltage of the NVPF/HC cell as a function of SoC at 25 °C. The black curve represents the OCV. The red, yellow and blue curves represent the simulated voltages of the cell when discharged respectively at -C/2, -1C and -2C. The dashed curves are the voltage measurements $U_{cell,meas}$ obtained from the tests.

ΔSoC_{sd} is determined by the difference between the SoC at which the measured voltage goes to 3.65 V and the SoC at which the OCV goes to 3.65 V. ΔSoC_{sd} is thus determined for each current tested. Afterwards, we adjusted the ΔSoC_{sd} measurements with (8), which gave values of 20.913 for k_1 and -1.177 for k_2. Fitting (1) to $U_{cell,meas}$, we found that R_{ld} equals 18 mΩ and τ_d equals 100 s at 25 °C.

When the SoC is above 30%, the simulated and measured voltages have almost the same shape. Thus, our model can predict the cell voltage for continuous discharges and SoC above 30%. The model is also able to predict the behavior of the battery after the one-hour pause at SoC close to 60%.

On the other hand, the proposed model cannot predict how the NVPF/HC cell reacts at SoC below 30%. This may be due to the limitation of the model by a ΔSoC_{sd} that doesn't take into account the difference of the complex mechanisms present in positive and negative electrodes [12], [17].

The model accurately predict the sharp voltage drop between SoC 40% and 50% at -C/2 and -1C. In the case where the current regime is -2C (blue curve in Fig. 5), the model was not able to track the voltage drop accurately. This may be linked to the heterogeneity of the SoC at large current regimes [18], which we did not study for this work.

C. Contribution of the model

This modeling approach shows promising results. First, it requires a much smaller number of tests than those needed for interpolation tables. With this approach, we characterized all model parameters using just three temperatures, three SoC and ten currents. This is too limited if we use the same number of tests to build efficient interpolation tables.

In addition, with this model, we have simplified the non-linearities in SoC, notably those of the diffusion parameters. Instead of using an equivalent diffusion impedance with strong non-linearies in SoC, it can be separated into solid and liquid diffusion that do not depend on SoC.

Moreover, with this new approach, the influence of temperature on the ECM parameters is modeled by Arrhenius equations. This avoids the need to interpolate and extrapolate parameters using interpolation tables. Actually, the influence of temperature characterized by linear equations can undermine the accuracy of the model.

VI. Conclusion

We have implemented a modified equivalent circuit model for NVPF/HC sodium-ion batteries. This model is easy to be embedded in the battery management software. Instead of using interpolation tables, we propose methods to characterize the model parameters using physics-based or behavioral equations. With these characterization methods, the model was able to predict the behavior of the cell taking into account the non-linearities of the present electrochemical phenomena.

The model is capable of providing information on the effects of charge transfers and the SEI as a function of current, temperature and SoC. As a result, the diagnosis of the charge transfers and the SEI may be possible. The model is also able to represent the effects of diffusion at SoC above 30%. It also distinguishes between the effects of sodium diffusion within the electrodes and sodium ion diffusion in the electrolyte. However, the model could not accurately predict the behavior of the battery at low SoC. This might be the result of not taking into account the particularities of each electrode. It might also be due to the usage of a homogeneous model whose accuracy is limited particularly with high currents [18].

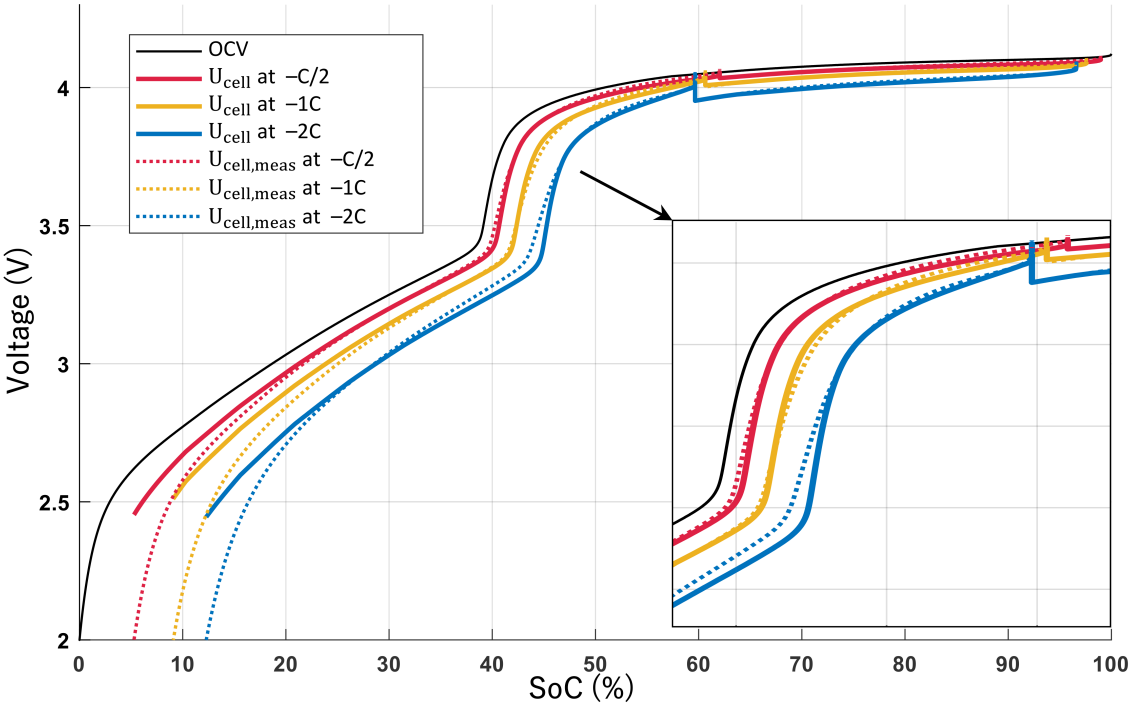

Fig. 5. Cell Voltages as a function of SoC at 25 °C and at current regimes of -C/2 (red), -1C (yellow) and -2C (blue).

In future work, the model may be modified so that it takes into account the heterogeneities in SoC, this may solve the accuracy problems at low SoC. Additionally, a state of health dependency may be added to the model.

ACKNOWLEDGMENT

The authors gratefully acknowledge the financial support from Région Hauts-de-France and Tiamat Energy.

REFERENCES

[1] J.-M. Tarascon, "Na-ion vs. Li-ion Batteries: complementarity rather than competitiveness," Joule, Vol.4 (8), pp.1616–1620, 2020.

[2] F. Dhaussy, J. T. Canh, Y. Raynaud, A. El-Mejdoubi, "High Power Battery Systems for Mild-Hybrid with Sodium-ion cobalt free technology," 2022.

[3] H. Rabab, N. Damay, F. Vendrame, C. Forgez, and A. El-Mejdoubi, "Modeling the non-linearities of charge-transfers and solid electrolyte interphase resistances for a sodium-ion battery with a hard carbon electrode," Electrimacs, 2022, in press.

[4] D. Andre, M. Meiler, K. Steiner, H. Walz, T. Soczka-Guth, and D.U. Sauer, "Characterization of high-power lithium-ion batteries by electrochemical impedance spectroscopy. II: Modelling," Journal of Power Sources, Vol. 196, pp. 5349–5356, 2011.

[5] S. Raël, and M. Hinaje, "Using electrical analogy to describe mass and charge transport in lithium-ion batteries," Journal of Power Sources, Vol. 222, pp. 112–122, 2013.

[6] N. Damay, C. Forgez, G. Friedrich, and M.-P. Bichat, "Heterogeneous behavior modeling of a LiFePO4-graphite cell using an equivalent electrical circuit," Journal of Energy Storage, vol. 12, pp. 167–177, 2017.

[7] M. Farkhondeh, M. Safari, M. Pritzker, M. Fowler, T. Han, J. Wang and C. Delacourt, "Full-Range Simulation of a Commercial LiFePO 4 Electrode Accounting for Bulk and Surface Effects: A Comparative Analysis ," Journal of The Electrochemical Society, vol. 161, pp. A201–A212, 2014.

[8] M. Juston, N. Damay, and C. Forgez, "Extracting the diffusion resistance and dynamic of a battery using pulse tests," Journal of Energy Storage, vol. 57, 2023.

[9] M. J. Lain, and E. Kendrick, "Understanding the limitations of lithium ion batteries at high rates," Journal of Power Sources, vol. 493, 2021.

[10] L. Gagneur, A.L. Driemeyer-Franco, C. Forgez, and G. Friedrich, "Modeling of the diffusion phenomenon in a lithium-ion cell using frequency or time domain identification," Microelectronics Reliability, vol. 53, pp. 784–796, 2013.

[11] N. Damay, K. Mergo Mbeya, G. Friedrich, and C. Forgez, "Separation of the charge transfers and solid electrolyte interphase contributions to a battery voltage by modeling their non-linearities regarding current and temperature," Journal of Power Sources, vol. 516, 2021.

[12] K. Chayambuka, G. Mulder, D.L. Danilov, and P.H.L. Notten, "Determination of state-of-charge dependent diffusion coefficients and kinetic rate constants of phase changing electrode materials using physics-based models," Journal of Power Sources Advances, vol. 9, 2021.

[13] F. Kremer, S. Rael, and M. Urbain, "1D electrochemical model of lithium-ion battery for a sizing methodology of thermal power plant integrated storage system," AIMS Energy, vol. 8, pp. 721–748, 2020.

[14] K. Mergo Mbeya, N. Damay, G. Friedrich, C. Forgez and M. Juston, "Off-line method to determine the electrode balancing of Li-ion batteries," Mathematics and Computers in Simulation, vol. 183, pp. 34–47, 2021.

[15] E. Kuhn, C. Forgez, P. Lagonotte and G. Friedrich, "Modelling Ni-mH battery using Cauer and Foster structures," Journal of Power Sources, vol. 158, pp. 1490–1497, 2006.

[16] P. Mauracher, and E. Karden, "Dynamic modelling of lead/acid batteries using impedance spectroscopy for parameter identification," Journal of Power Sources, vol. 67, pp. 69–84, 1997.

[17] C. M. Ghimbeu, J. Górka, V. Simone, L. Simonin, S. Martinet, and C. Vix-Guterl, "Insights on the Na^+ ion storage mechanism in hard carbon: discrimination between the porosity, surface functional groups and defects," Nano energy, Vol. 44, pp. 327–335, 2018.

[18] M. Juston, N. Damay, C. Forgez, G. Friedrich, S. Vivier, K. Mergo Mbeya, and B. Vulturescu, "Direct determination of a single battery internal resistances distribution using a heterogeneous model," Mathematics and Computers in Simulation, vol. 183, pp. 20–33, 2021.